Current Research in Green and Sustainable Chemistry 4 (2021) 100110

Contents lists available at ScienceDirect

Current Research in Green and Sustainable Chemistry

journal homepage: www.elsevier.com/journals/current-research-in-green-and-sustainable-chemistry/2666-0865

Rod-like L-Aspartic acid-Cu(II) metal organic frameworks; Synthesis, characterization and biomedical properties

Gorkem Gizer [a], Mehtap Sahiner [b], Yildiz Yildirim [c], Sahin Demirci [a], Mehmet Can [a], Nurettin Sahiner [a,d,e,*]

[a] Canakkale Onsekiz Mart University, Faculty of Science and Arts, Department of Chemistry & Nanoscience and Technology Research and Application Center (NANORAC), Terzioglu Campus, Canakkale, 17100, Turkey
[b] Canakkale Onsekiz Mart University, Terzioglu, Canakkale School of Applied Science, Department of Fashion Design, Terzioglu Campus, 17100, Canakkale, Turkey
[c] Kaleseram R&D Ctr, Can, Canakkale, Turkey
[d] Department of Chemical and Biomolecular Engineering, University of South Florida, Tampa, FL, 33620, USA
[e] Department of Ophthalmology, Morsani College of Medicine, University of South Florida, 12901 Bruce B. Downs Blvd, MDC21, Tampa, FL, 33612, USA

ARTICLE INFO

Keywords:
L-aspartic acid
porous Coordination network
Bio-MOF
Blood compatible
Antimicrobial
Antidiabetic

ABSTRACT

L-aspartic acid (L-AA) based MOFs were prepared from acetate, chloride, nitrate, and sulfate salts of Cu(II) ions as L-AA-Cu(II)-A,-C,-N,-S, respectively with 96.7 ± 2.4, 89.8 ± 3.1, 92.1 ± 1.5, 74.6 ± 5.2 m^2/g, surface areas. L-AA-Cu(II)-MOFs in the same order induced 0.43 ± 0.25%, 0.94 ± 0.24%, 0.91 ± 0.40%, 1.18 ± 0.10% hemolysis, all being <2%, and blood clotting indices of ~90% and can be considered nonhemolytic and non-coagulative at 1 μg/mL concentration. L-AA-Cu(II)-A MOFs exhibited 86.3 ± 0.2, and 92.4 ± 0.6% α-Glucosidase inhibitory activities at 1.0 and 10.0 μg/mL concentrations, respectively. Moreover, L-AA-Cu(II)-S MOFs had effective antimicrobial activities against *E. coli* (ATCC-8739), and *S. aureus* (ATCC-6538) with MIC values of 0.63 mg/mL and 1.25 mg/mL for *C. albicans* (ATCC-10231). L-AA-Cu(II) MOFs synthesized herein with hemocompatible, antimicrobial and antidiabetic properties prompt interesting possibilities for both industrial and biomedical applications.

1. Introduction

Metal-organic frameworks (MOFs), also known as porous coordination networks (PCNs), are sophisticated products of material science, considerably captured scientific interest in the last two decades [1]. Enormous accessible internal surface areas, high void volumes, and numerous chances of metal and organic ligand combinations as well as finely adjustable structural properties of MOFs through pre-, and post synthetic approaches bestow them unprecedented versatility to target vast array of applications in biological and industrial realms [1–3]. Not only the extraordinary topology and structural properties of MOFs exert potent functionalities but also the flexibility in synthesis and modification methodologies provide great opportunity to design tailor-made unique MOF structures demanded in broad spectrum of applications from supercapacitor [4], and catalysis applications [5], carbon capture [6], gas absorption and storage technologies [7,8] to magnetic and molecular separation [9], biosensing [10], bioimaging [11], drug delivery [12], and much more. Solvent evaporation method [13], diffusion method [14], hydro(solvo) thermal method [15,16], microwave reaction and ultrasonic method [17], stand out some of the most preferred methodologies in synthesis of MOFs. Although most of the industrial MOFs are comprised of toxic metal ions and organic ligands, those formulations intended for biomedical applications require biocompatibility and safety as primary criteria [18]. Hence, meticulous attempts on integrating MOFs into biomedical applications together with urging quest for environment friendly MOFs in industry have led to exploration of biocompatible, non-toxic, or relatively as much lowest-toxicity metal and ligand combinations for construction of innocuous coordination architectures so called “green MOFs” [19]. In this context, MOFs designed from biological molecules (bio-ligands) such as saccharides [20], amino acids [3,21], peptides [22–24], nucleobases [25–27], and phenolic compounds [28–31] opened up a solid-step-forward novel insights in development of MOF materials not only for their biocompatibility, but they also offered added advantage to employ inherent functionality of

* Corresponding author. Canakkale Onsekiz Mart University, Faculty of Science and Arts, Department of Chemistry & Nanoscience and Technology Research and Application Center (NANORAC), Terzioglu Campus, Canakkale, 17100, Turkey.
E-mail address: sahiner71@gmail.com (N. Sahiner).

https://doi.org/10.1016/j.crgsc.2021.100110
Received 2 April 2021; Received in revised form 3 May 2021; Accepted 3 May 2021
Available online 7 May 2021

biomolecules. The benefits of utilizing functional biomolecules are multiple coordination sites, multidentate coordination modes, chirality, aliphatic/cyclic backbone functionalities, self-assembly properties, facile modifiability, hydrogen bonding, ionic and π–π stacking interactions [3,19], along with natural abundance and amenable commercial availability in bulk quantities.

Amongst the a forecited biomolecules, amino acids are one of the most important bio-ligands in bio-MOF formulations [19]. They are the smallest functional units of proteins dictating their interactions with other molecules through noncovalent weak interactions via their carboxylate and amino groups serving as metal chelation/complexing sites [32]. Also, various side groups of amino acids with different characters such as charged, hydrophilic/hydrophobic, or aliphatic/aromatic moieties are employed as binding sites for metal ions hence, aid maintaining protein functions [33].

Numerous MOF preparations with different metal ions have been formulated from various amino acids including, L-tryptophan [34], L-glutamic acid [35], L-glutamine [36], L-alanine [37], L-tyrosine [38], L-serine [39], L-glycine [40], L-histidine [41], and L-aspartic acid [42].

L-aspartic acid is a non-essential, yet a pivotal α-amino acid involved in many biological tasks such as participating cellular energy production, synthesis of other biomolecules and proteins [43], inhibition of β-Glucuronidase in blockage of enterohepatic bilirubin circulation [44], and antagonizing effects on inhibition of L-asparaginase activity of morphine in brain [45], and so forth used for treatment of opiate addiction [46], hypertension, hepatopathy and heart diseases [47]. Not only can L-aspartic acid function as a multifunctional biomolecule in metabolic processes, but it has also been considered an interested molecule from chemical point of view due mainly to possessing three potential donor sites conveniently allows for development of versatile coordination complexes [32,48,49].

In this study, L-aspartic acid (L-AA) has been chosen as a natural-based organic ligand (bioligand) and different salts of Cu(II) ion such as Cu(II) acetate (-A), Cu(II) chloride (-C), Cu(II) nitrate (-N), Cu(II) sulfate (-S), as metal linkers were used to prepare L-AA-Cu(II)-A, L-AA-Cu(II)-C, L-AA-Cu(II)-N, and L-AA-Cu(II)-S MOFs. Structural, morphological, compositional, and surface characterization of the L-AA-Cu(II) MOFs were caried out by X-Ray diffraction (XRD), Fourier transform infrared (FT-IR) spectroscopy, atomic absorption spectroscopy (AAS), thermogravimetric analysis (TGA), scanning electron microscopy (SEM), and Brunauer–Emmett–Teller (BET) N_2 adsorption/desorption analyses. In order to evaluate the biomedical potential of L-AA based Cu(II) MOFs, blood compatibility tested via *in vitro* hemolysis and blood clotting assays were investigated. Also, α-Glucosidase inhibitory activity of L-AA based Cu MOFs were evaluated to determine their antidiabetic potential. Furthermore, antimicrobial properties of L-AA-Cu(II) MOFs were explored against gram (−) *E. coli* (ATCC 8739), gram (+), *S. aureus* (ATCC 6538) bacteria and *C. albicans* (ATCC 10231)) fungal strains to reveal their antimicrobial capacity for both biomedical and industrial application potentials.

2. Experimental

2.1. Materials

The L(+)-Aspartic acid (L-AA, 98%, Acros) was used as bridging bioligand, and copper acetate monohydrate ($CuCH_3COOH.H_2O$, 98%, Sigma Aldrich), copper chloride anhydrous ($CuCl_2$, 99%, Kimetsan), copper nitrate hexahydrate ($Cu(NO_3)_2.6H_2O$, 98%, Fluka), and copper sulfate pentahydrate ($Cu(SO_4)_2.5H_2O$, 99%, Sigma Aldrich) metal salts were used as sources of Cu(II) ions in synthesis of L-AA-Cu(II) MOFs. Sodium hydroxide (NaOH, 99%, Merck) and hydrochloric acid (HCl, 36.5%, WVR Chemicals) were used in pH adjustments of L-AA aqueous solutions. Sodium chloride (NaCl, 99%, Sigma Aldric), and calcium chloride ($CaCl_2$, 99%, Merck) were used in blood compatibility assays. The α-Glucosidase from *Saccharomyces cerevisiae* (EC Number: 3.2.1.20, 10 units/mg protein, Sigma Aldrich), and 4-nitrophenyl α-D-glucopyranoside (4-NPG, 99%, Acros) as a calorimetric substrate for α-Glucosidase were used in enzyme inhibition studies.

2.2. Synthesis of L-AA-Cu(II) MOFs with different anion source

The synthesis of L-AA based MOFs was accomplished in aqueous medium following the literature with small changes [50]. In brief, a 100 mL beaker was charged with 1.0 g of L-AA and dissolved in 50 mL of double-distilled water (DDw) at 500 rpm stirring via occasional addition of 1 M NaOH solution. After complete dissolution of L-AA, the pH of solution was adjusted to 7.0 by using 1 M HCl solution. Then, the aqueous solutions of Cu (II) prepared from acetate, chloride, nitrate, and sulfate salts containing stoichiometrically 1:1 mol ratio of Cu(II) ions with respect to L-AA were added drop-by-drop into different L-AA solutions at pH 7 and stirred at 750 rpm mixing for 12 h. Afterwards, blue colored solid assemblies (L-AA based Cu(II) MOFs) formed during the reaction were filtered and washed in sequence with water, water-ethanol (1:1 v/v), and water, then lyophilized to dryness via a freeze-dryer and stored in closed tubes until further usage. L-AA-Cu(II) MOFs were named according to Cu(II) sources used as L-AA-Cu(II)-A, L-AA-Cu(II)-C, L-AA-Cu(II)-N, and L-AA-Cu(II)-S, respectively for acetate, chloride, nitrate, and sulfate salts of copper.

2.3. Characterization of Cu(II) based MOFs

The scanning electron microscope (SEM, 400F Field Emission SEM, Quanta) was used for the visual characterization of L-AA based Cu(II) MOFs' morphology. For this purpose, certain amounts of dry samples mounted on SEM stubs were sputtered in gold an imaging was performed under vacuum at 30.00 kV operation voltage.

X-ray powder diffraction patterns of the L-AA and L-AA based Cu(II) MOFs were recorded by a PANalytical X'Pert Pro MPD diffractometer equipped with CuKα radiation and the X'Celerator detector on diffracted beam [51]. The XRD data were collected in a Bragg Brentano (θ/θ) vertical geometry operating in flat reflection mode between 3° and 70° (2θ) in steps of 0.02° 2θ with 1 s step-counting time. The X-ray tube operating at 40 mA, 45 kV was used and 1/2° divergence slit with a 0.04 rad soller slit and a 10 mm fixed mask was placed in the incident beam pathway. The raw powder diffraction data was processed with High Score Plus (v.4.6.0) software, for peak identification and analyses of diffraction peaks by automated search-match calculation. Schematic crystallographic structure of L-AA-Cu(II) MOF was modelled by Cortona3D software.

The FT-IR spectra (Spectrum, PerkinElmer) of L-AA based Cu(II) MOFs were recorded in the range of 4000-650 cm^{-1} wavenumbers at 4 cm^{-1} peak resolution, and the average of four internal scans were collected by attenuated total reflection (ATR) method.

Thermal behaviors of L-AA based Cu(II) MOFs were characterized by a thermogravimetric analyzer (TGA, SII 6300, Exstar). Briefly, certain amounts of MOF samples were placed into TGA pans and heated up to 100 °C under flow of 200 mL/min N_2 gas at 10 °C/min heating rate and held for 15 min to eliminate moisture and then were heated up to 1000 °C. TGA curves of L-AA-Cu(II) MOFs were constructed by plotting cumulative weight loss against temperature, the effect of Cu(II) source on thermal stability of MOFs was compared.

Atomic absorption spectrometer (AAS, iCE 3000, Thermo) was used for the determination of metal ion content of L-AA based Cu(II) MOFs. Shortly, 50 mg of each type of MOF samples were placed into 40 mL of 5 M HCl solution and stirred for 4 h for the disassembly of coordination bonds and, Cu(II) ion contents were determined by AAS from the previously constructed Cu(II) calibration curve.

Porosity and surface properties of L-AA-Cu(II) MOFs were characterized by a surface area and porosity analyzer (TriStar II, Micromeritics) based on N_2 adsorption/desorption kinetics using BET and BJH methods. Briefly, MOF samples were degassed with N_2 gas for 12 h before analysis,

and N_2 gas adsorption/desorption curves were obtained under liquid nitrogen environment.

2.4. α-Glucosidase inhibition studies

L-AA based Cu(II) MOFs were investigated for their potential inhibitory effects on α-Glucosidase enzyme by following the reported enzyme assay in literature [52]. 4-NPG as a colorimetric substrate of α-Glucosidase was used for determination of enzymatic activity. The inhibition assay was performed via a microplate reader (Multiskan Sky, Thermo) at the wavelength of 405 nm, the amount of 4-NP as an end-product of enzymatic reaction was quantified and compared with the control group lacking MOF samples. All four types of L-AA based Cu(II) MOFs at 10 μg/mL concentration were used for enzyme inhibition assay and the L-AA-Cu(II)-A MOFs with the highest inhibition effect was further investigated for its concentration dependent activity at 0.25, 1, 5, 10, and 25 μg/mL concentrations.

2.5. Antimicrobial properties

The antimicrobial activities of L-AA-Cu(II) MOFs against *E. coli* (gram -, ATCC 8739), *S. aureus* (gram +, ATCC 6538) and *C. albicans* (fungi, ATCC 10231) were investigated via micro-dilution method [53]. Specifically, 10 mg of different types of L-AA-Cu(II) MOFs were suspended in 10 mL of IS solutions to achieve a final concentration of 1 mg/mL. Afterwards, the sample suspensions were sterilized under UV light at 420 nm for 1 min. Then, the bacterial and fungal strains revived from −20 °C stock at room temperature (20 °C) 24 h prior to experiment were adjusted for turbidity as nearly 1×10^8 colony forming unit per mL (CFU/mL) for each according to McFarland 0.5 standard. Then, different concentrations of samples from 0.312 mg/mL to 1 mg/mL were added into 2 mL of nutrient broth media, and 20 μL of each microorganism suspension was inoculated in sample containing liquid media. After then, microorganisms were incubated at 35 °C for 18–24 h. After the incubation, 100 μL of each inoculum was seeded on separate nutrient agar plates with proper dilutions using IS solution wherever necessary and then incubated for 24 h more at 35 °C. Afterwards, survivors of bacterial and fungal colonies were counted to quantify minimum inhibition concentration (MIC) and minimum bactericidal/fungal concentration (MBC, MFC) activities of L-AA based Cu(II) MOFs.

2.6. Blood compatibility studies

Blood compatibility of the L-AA based Cu(II) MOFs were evaluated by *in vitro* hemolysis and blood clotting assays according to literature with minor alterations [53]. Hemocompatibility assays were performed after the institutional approval from the Human Research Ethics Committee of Canakkale Onsekiz Mart University (2011-KAEK-27/2020-E.2000045671). Human whole blood was used for the assays, and the blood specimens were freshly obtained from healthy unmedicated people via vacutainer syringes and then preserved in vacutainers containing anticoagulant EDTA to inhibit clotting. Both hemolysis and clotting assays were performed at final sample concentrations of 1 μg/mL prepared by suspending L-AA Cu(II) MOFs in 0.9% isotonic saline (IS) solution.

2.7. Hemolysis test

For the assessment of % hemolytic ratio induced by L-AA based Cu-MOFs, 10 μL of 1000 μg/mL sample suspensions prepared in IS solution was further diluted up to 9.8 mL and incubated at 37.5 °C for 15 min. Meanwhile, 2 mL of anticoagulated blood was diluted with 2.5 mL of IS and 0.2 mL of this blood solution was added into sample tubes, mixed by gentle inversion and then incubated for 1 h at 37.5 °C in a shaking water bath. Positive and negative control groups were set by incubating 0.2 mL of diluted blood in only DDw and IS solution, respectively. At the end of incubation process, 1.5 mL aliquots of blood-MOF suspensions and controls were taken and centrifuged at 1340 rpm for 5 min. Afterwards supernatants of samples were carefully aspirated into UV–Vis cuvettes and absorbance values were measured at 542 nm. The hemolysis% ratio was calculated from Eq. (1) given below:

$$Hemolysis\ (\%) = \frac{\left(A_{542}^{sample} - A_{542}^{Negative}\right)}{\left(A_{542}^{Positive} - A_{542}^{Negative}\right)} \times 100 \quad (1)$$

Where A_{542}^{sample} is the absorbance of blood-MOF suspension, $A_{542}^{Negative}$ and $A_{542}^{Positive}$ are absorbances of respectively only blood-IS and only blood-DDw solutions, respectively.

2.8. Blood clotting test

The blood clotting capacity of L-AA-Cu(II) MOFs were assessed via blood clotting assay. Concisely, 10 μL of 1000 μg/mL sample suspensions prepared in IS solution were placed into falcon tubes and placed into a shaking water bath at 37.5 °C for 15 min incubation. Then, recording the time in a synchronous fashion, 3 mL of anticoagulated whole blood was mixed with 0.24 mL of 0.2 M freshly prepared $CaCl_2$ solution followed by immediate addition of 0.270 mL of $CaCl_2$ added blood on top of MOF samples in a way that entire portion of sample suspensions were covered by the added blood specimens. After incubation of samples at 37.5 °C for 10 min blood-sample mixtures were added 10 mL of DDw and centrifuged for 1 min at 540 rpm to precipitate potential clots that might possibly be developed depending upon the nature of materials. After centrifugation, fluid portion of blood was further diluted with 40 mL of DDw in a separate tube without transferring solid clots if formed. Finally, samples were incubated for 1 h at 37.5 °C before reading the absorbance values at 542 nm wavelength. As a control group, 0.270 mL of blood was mixed with 50 mL of DDw and assayed under the same conditions. The blood clotting index of MOF samples were calculated from Eq. (2):

$$Blood\ clottin\ index(\%) = \frac{\left(A_{542}^{sample}\right)}{\left(A_{542}^{Control}\right)} \times 100 \quad (2)$$

Where A_{542}^{Sample} and $A_{542}^{Control}$ are the absorbance values of blood-MOF suspensions and blood solution solely incubated by 50 mL of DDw, respectively.

3. Results and discussion

3.1. Synthesis and characterization of L-AA based amino acid Cu(II) MOFs

In our previous studies, we reported the synthesis, characterization, antimicrobial, and sensory properties of MOFs prepared by L-Glu as organic ligand, and Cu(II), Ni(II), and Co(II) ions as metal nodes [35]. In this investigation, another acidic amino acid, L-AA was pursued in the preparation of porous coordination networks (PON) in a greener synthesis methodology using different salts of Cu(II) ions as acetate (A), chloride (C), nitrate(N), and sulfate(S) and their effect on physicochemical properties of prepared MOFs was thoroughly investigated. L-AA is known to be negatively charged at physiological pH, the carboxyl groups of which are found in deprotonated form whereas the amino groups are in protonated state. Schematic illustration of L-AA based Cu(II) MOFs synthesis is given in Fig. 1 (a).

As seen from Fig. 1 (a), the carboxylate groups of L-AA and various salts of Cu(II) ions were electrostatically interacted to develop L-AA-Cu(II) coordination assemblies and blue colored solid phases were obtained after synthesis for all Cu(II) ion sources (data not shown).

SEM images of L-AA-Cu(II)-A, L-AA-Cu(II)-C, L-AA-Cu(II)-N, and L-AA-Cu(II)-S MOFs are given in Fig. 1 **(b)**. As can be easily noticed from the micrographs, all types of L-AA Cu(II) MOFs attained are similarly in

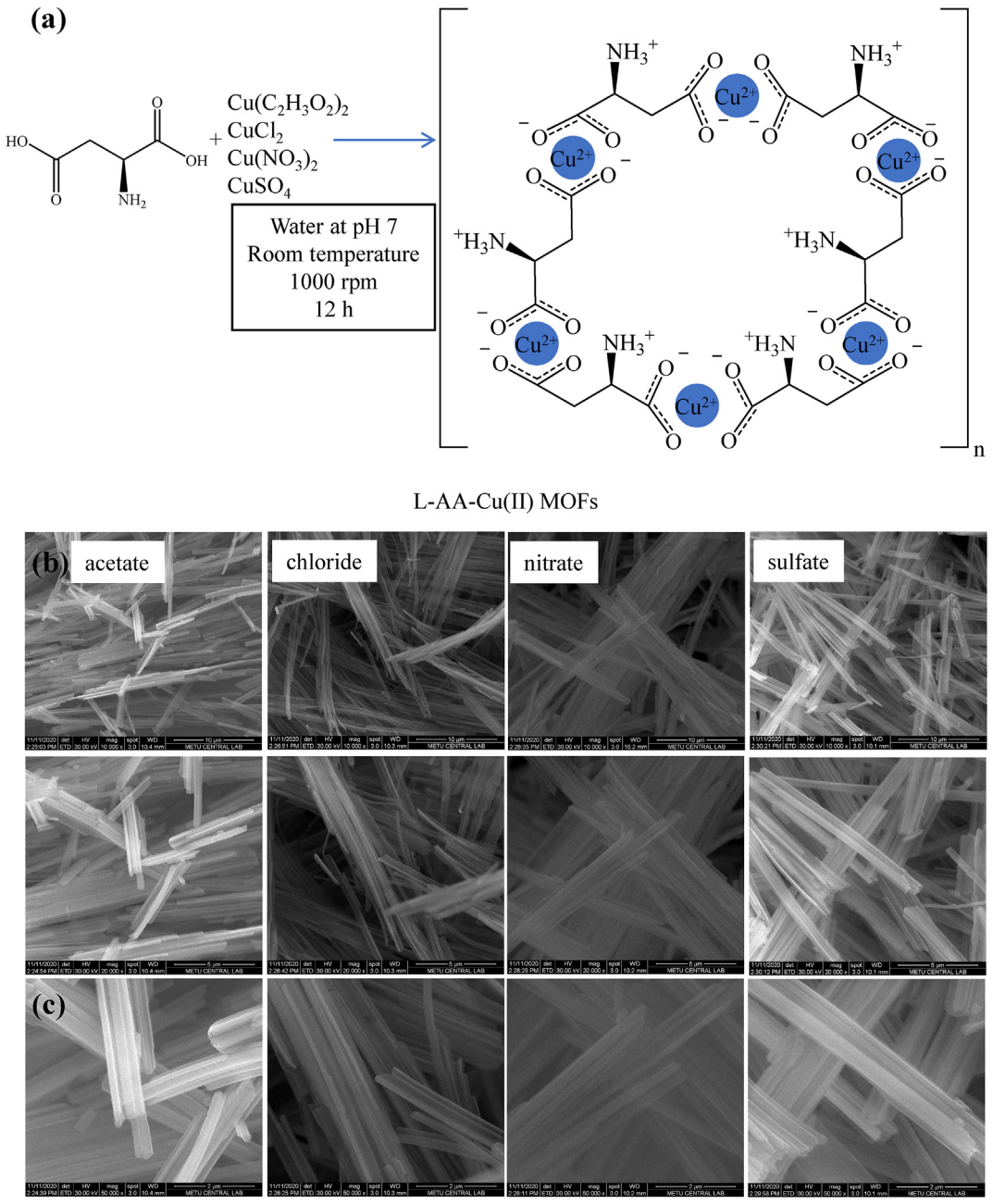

Fig. 1. **(a)** Schematic representation of L-AA based MOF synthesis, **(b)** long-shot and **(c)** closeup SEM images of the L-AA Cu(II) based MOFs prepared from different salts of Cu(II) ions.

rod-like or fiber-like morphologies and sizes range approximately 8–15 μm in length and 0.2–0.5 μm widths which can be more visibly realized from closeup SEM images (at 50,000X magnifications) given in Fig. 1 (c). Zhao et al. disclosed the influence of materials' shape on their potential for biomedical application [54]. In the study on mice, the retention times of materials of different shapes in stomach and intestine were assed and found that the retentions of rod-like structures in stomach and intestine were more than those of the spherical shaped structures [54]. Materials with rod-like morphology has also been reported to have several advantages such as effective, directed path for charge carriers [55], and minimal percolation thresholds [56]. These advantages of rod-like structures can be explained with their physical properties pertaining to aspect ratio, volume fraction, polydispersity and orientation [57].

The phase purity and crystallographic structures of native L-AA, and L-AA-Cu(II)-A, L-AA-Cu(II)-C, L-AA-Cu(II)-N, and L-AA-Cu(II)-S MOFs were characterized by XRD measurements and the obtained XRD patterns are demonstrated in Fig. 2 (a).

The main XRD peaks were observed at 11.7, 23.6, 35.8, and 37.1°2Θ with (0 0 1), (0 0 2), (0 0 3), and (1 0 3) planes, respectively. X-ray diffraction spectra of all types of L-AA-Cu(II) MOFs have shared the same peak positions with different intensities of diffractions. These intense diffraction peaks suggest the presence of good crystallinity in L-AA-Cu(II) coordination. The crystallinity of L-AA based Cu(II) MOFs was ranged from L-AA-Cu(II)-A to L-AA-Cu(II)-C, L-AA-Cu(II)-N, and L-AA-Cu(II)-S MOFs with respectively 81.5, 74.8, 76.4, and 50.2% crystalline characters. Fig. 2 (b) depicts schematic crystallographic structure of L-AA based Cu(II) MOFs. L-AA is an acidic amino acid with an amino and two carboxylate groups. Each of these functional groups can potentially be served as donor sites for metal centers. However, based on computationally constructed model dominant pattern on MOF formation follows

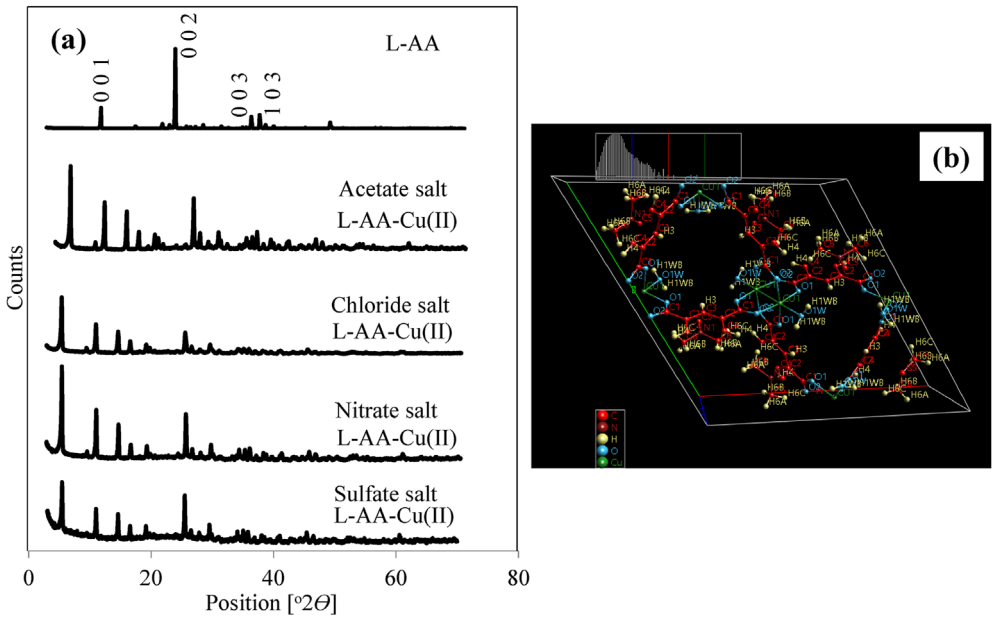

Fig. 2. (a) The XRD pattern of L-AA and L-AA based Cu(II) MOFs and **(b)** the illustration of coordination patterns between L-AA and Cu(II) ions obtained by computational modelling.

coordination of two carboxylate groups of L-AA with Cu(II) ions. Moreover, the crystallographic data for L-AA-Cu(II) MOF structures are summarized in Table S1. As seen from and Fig. 2 (b), the hexagonal crystallization was occurred for all types of L-AA-Cu(II) MOFs.

For the structural analysis, FT-IR spectra and TGA curves of L-AA-Cu(II) MOFs are respectively presented in Fig. 3 (a) and **(b)**, In the FT-IR spectrum of L-AA, the peaks at 1685 cm^{-1} were assigned to C=O stretching modes of carboxylic acid groups, and the peaks at 1501, and 1419 cm^{-1} were attributed to COOH stretching vibrations [58]. In addition, the FT-IR peaks recorded around 1640, and 1597 cm^{-1} were assigned to N-H stretching and bending frequencies of NH_2 groups, while the peaks appeared at 1149 and 1118 cm^{-1} were attributed to NH_2 rocking modes, respectively [58]. As can be seen from FT-IR spectra of all L-AA-Cu(II) based MOFs, it is worth noting to point out change and shifting the C=O peaks at 1685 cm^{-1} and maintenance of amine peaks in the MOF structure with red and blue shifts coherently validates computationally obtained crystallographic coordination model given in Fig. 2 (b), and hence supports formation of L-AA based Cu(II) MOFs through coordination of carboxylate groups with Cu(II) ions. Characterization of MOFs' thermal stability is another useful means of predicting their potential applications especially in industrial use [59]. Thermal degradation of L-AA based Cu(II) MOFs were given in Fig. 3 (b). From the TGA curve of native L-AA, it is seen that degradation was completed in 3 steps between 210 and 260, 360–415, and 480–640 °C with 25.4, 59.2, 98.8% weight losses, respectively and 99.2% of cumulative weight loss was observed at 1000 °C. On the other hand, the thermal stability of L-AA based Cu(II) MOFs were decreased as was seen to progress in 4 main degradation steps with similar trends except for slight differences at initial decomposition temperatures ranging from L-AA-Cu(II)-S to C, A and N in ascending order. Thermal degradation steps of L-AA based Cu(II) MOFs occurred between 100 and 150 °C, 200–240 °C, 300–390 °C, and 450–640 °C with approximately 5, 50, 60 and 65% weight losses, respectively.

The residual weight percent were determined as nearly 35% for all L-AA-Cu(II) MOFs and composition of the remainders were anticipated to contain Cu_2O residues [60]. Moreover, the amount of Cu(II) ions contained by L-AA based MOFs were determined via AAS and calculated yield%, as well as gravimetric amounts of Cu(II) ions based on AAS analysis are summarized in Table 1.

The amount of Cu(II) ions per gram of L-AA based Cu(II) MOFs were found to be almost similar for all types as 239.3 ± 15.9, 254.9 ± 11.6, 257.1 ± 16.2, and 239.2 ± 14.8 mg/g for L-AA-Cu(II)-A, L-AA-Cu(II)-C, L-AA-Cu(II)-N, and L-AA-Cu(II)-S MOFs, respectively and the yield% was calculated as 40.5 ± 2.1, 50.8 ± 1.9, 40.2 ± 1.6, and 36.8 ± 1.3% in the same order.

The surface and porosity of the L-AA-Cu(II) MOFs were investigated via N_2 adsorption/desorption measurements and corresponding isotherms were given in Fig. 4 (a). N_2 adsorption/desorption curves of all L-AA-Cu(II)-A, L-AA-Cu(II)-C, L-AA-Cu(II)-N, and L-AA-Cu(II)-S MOFs have shown to exhibit characteristics of type II isotherms and H4 type hysteresis loops suggesting presence of narrow slit-like mesopores in the MOF structures [61].

The plots given in Fig. 4 (b) illustrates distribution of the pore size in the structure of L-AA based Cu(II) MOFs where two kinds of pore sizes can be clearly identified in all types of L-AA Cu(II) MOFs around 50 to 60 A^o for L-AA-Cu(II)-A, L-AA-Cu(II)-C, and L-AA-Cu(II)-N MOFs whereas slightly lower pore size have seen in L-AA-Cu(II)-S MOFs around 40 A^o.

The average S_{BET} surface areas, pore sizes and volumes of L-AA-Cu(II) MOFs were summarized in Table 1. As seen from the results of S_{BET} analysis, almost similar surface areas were obtained for L-AA-Cu(II)-A, L-AA-Cu(II)-C, and L-AA-Cu(II)-N MOFs with respectively 96.7 ± 2.4, 89.8 ± 3.1, 92.1 ± 1.5 m^2/g, and a lower surface area of 74.6 ± 5.2 m^2/g for L-AA-Cu(II)-S MOFs. Based on these findings, it is plausible to reach a conclusion that the S_{BET} data gave supportive results with Fig. 4. The magnitude of average pore volumes for all L-AA-Cu(II) MOFs were found between 0.25 and 0.29 cm^3/g and, the average pore sizes for L-AA-Cu(II)-A, L-AA-Cu(II)-C, L-AA-Cu(II)-N, and L-AA-Cu(II)-S MOFs were measured as 6.4 ± 0.2, 7.7 ± 0.2, 6.9 ± 0.1, and 8.3 ± 0.6 nm, respectively. Therefore, all the prepared L-AA-Cu(II) are mesoporous materials.

3.2. α-Glucosidase enzyme inhibition capability of L-AA-Cu(II) based MOFs

The inhibition of α-Glucosidase enzyme has attracted great attention due to its treatment potential on type II diabetes and hyperglycemia in a controllable manner [62]. Controllable inhibition of α-Glucosidase enzyme provides a chance for balancing blood sugar levels and help ameliorating deleterious effects of type II diabetes and associated with hyperglycemia [63]. Many researchers investigated the inhibition of α-Glucosidase enzyme in the treatment type II diabetes to enhance

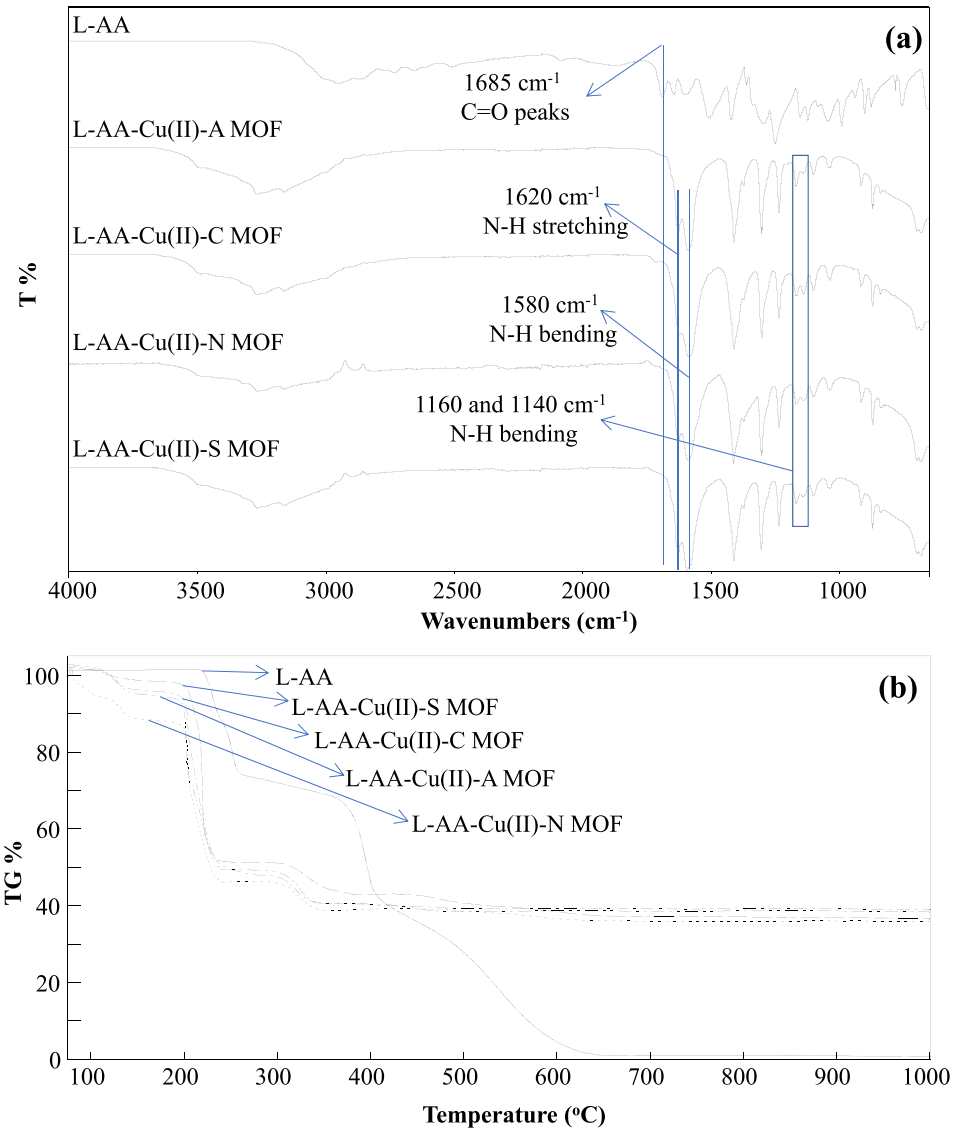

Figure 3. Comparison of **(a)** the FT-IR spectra and **(b)** TGA graphs of native L-AA, and L-AA based Cu(II) MOFs.

Fig. 3. Comparison of **(a)** the FT-IR spectra and **(b)** TGA graphs of native L-AA, and L-AA based Cu(II) MOFs.

Table 1
Cu(II) ion contents, gravimetric yields (%), surface and porosity properties of L-AA-Cu(II) MOFs.

MOFs	Cu(II) salts of	Amount of Cu(II) (mg/g)	Yield%	Surface Area (m^2/g)	Pore volume (cm^3/g)	Pore Size (nm)
L-AA-Cu(II)	**Acetate**	239.3 ± 15.9	40.5 ± 2.1	96.7 ± 2.4	0.25 ± 0.01	6.4 ± 0.2
	Chloride	254.9 ± 11.6	50.8 ± 1.9	89.8 ± 3.1	0.29 ± 0.01	7.7 ± 0.2
	Nitrate	257.1 ± 16.2	40.2 ± 1.6	92.1 ± 1.5	0.29 ± 0.02	6.9 ± 0.1
	Sulfate	239.2 ± 14.8	36.8 ± 1.3	74.6 ± 5.2	0.25 ± 0.01	8.3 ± 0.6

therapeutic efficacy [64–67]. MOFs are reported to interact with enzymes through hydrogen bonding, electrostatic, and van der Waals forces [68,69]. Many Cu (II) based MOFs synthesized using various ligands such as nitrogen containing ligands, insulin mimetic ligands or mixed ligand complexes have been reported for their a-Glu inhibitory activities [70–72]. L-AA was ported to be present and in active sites of α-Glucosidase and other homology modelled analog enzymes [73] together with other amino acids such as arginine, glutamic acid, and histidine residues [74].

Here, considering the function of L-AA in α-Glucosidase enzyme and the strong coordination ability of Cu (II) ions with L-AA [32] as well as with the other amino acids [35,75] that is present in the active site of the enzyme, the α-Glucosidase inhibitory activity of L-AA based Cu(II) MOFs prepared from different metal ion sources were investigated at 10 μg/mL concentration and the results are demonstrated in Fig. 5 (a). It was clearly seen from Fig. 5 (a) that, L-AA based Cu(II) MOFs achieved approximately 90% inhibition activity at 10 μg/mL concentration.

Specifically, inhibitory activities of L-AA-Cu(II)-A, L-AA-Cu(II)-C, L-AA-Cu(II)-N, and L-AA-Cu(II)-S MOFs were found to be 92.4 ± 0.6, 91.5 ± 0.3, 90.3 ± 1.3, and 90.1 ± 1.7%, respectively. Almost entirely

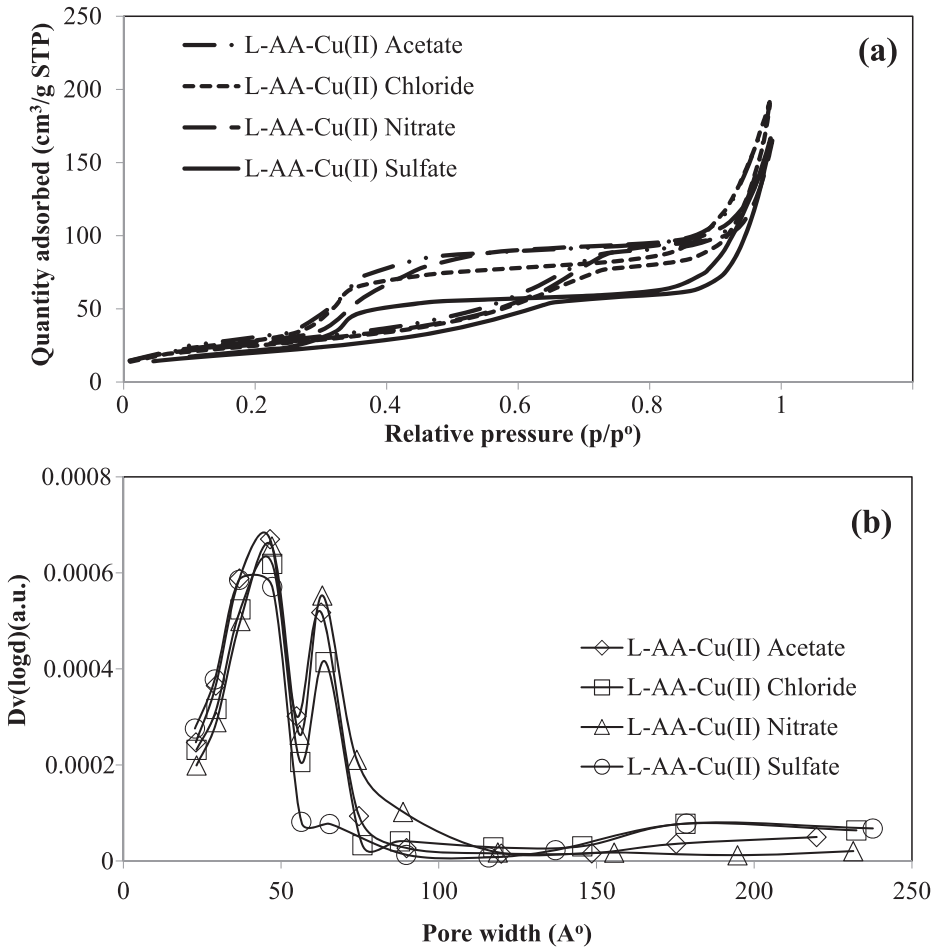

Fig. 4. **(a)**The N_2 gas adsorption/desorption isotherms and **(b)** pore size distribution plots of L-AA based Cu(II) MOFs.

inhibition of α-Glucosidase by L-AA based Cu(II) MOFs even at as low as 10 μg/mL concentrations highlights their potency in development of potential therapeutics thereof. On the other hand, concentration-dependent inhibition study performed on L-AA-Cu(II)-A MOFs revealed preservation of about 50% inhibition activity even after 40 folds of dilution (0.25 μg/mL). Affectedly, as can be seen from Fig. 5 (b), the concentration dependence of L-AA-Cu(II)-A MOFs in 0.25–25 μg/mL range revealed 50.8 ± 0.9, 68.7 ± 0.3, 86.3 ± 0.2, 92.4 ± 0.6, and 92.7 ± 0.2% inhibition capability. This result corroborates that the L-AA-Cu(II)-A can be potentially used in the treatments of type II diabetes at ≥25 μg/mL with over 90% inhibition of α-Glucosidase enzyme. However, more elaborate experimental or computational analyses on the binding modes, and affinities to characterize detailed mechanism of α-Glucosidase inhibition need to be studied.

3.3. Antimicrobial properties of L-AA-Cu(II) MOFs

In the literature, the antibacterial activities of MOFs have been described in two possible routes such as by the action of metal ions leached from MOF crystals interfering with the ion transport system and enzymatic activities of bacteria or through loss of bacterial cell wall integrity by the active metal sites of MOFs which are known to disrupt the bacterial membrane and cause outflow of the cytoplasmic contents [76]. In a study reported by Zhuang et al., the Co (II)-based MOF, $[Co_4(H_2O)_2(TDM)\ (H_2O)_8]$ (Co-TDM, TDM8− =[(3,5-dicarboxyphenyl)-oxamethyl] methane), were revealed to exert effective bactericidal activity against *E. coli* [76]. Lu et al., reported the higher antibacterial activities of three-dimensional Ag-MOFs than the commercial silver (Ag) NPs [76]. Furthermore, Rodríguez et al., reported that the crystals of HKUST-1 (=MOF-199), $[Cu_3(BTC)_2(H_2O)_3]n$ where BTC is 1,3,5-benzenetricarboxylate, immobilized on cellulose fibers have had very good antibacterial activity against *E. coli* [76]. Moreover, four different Cu(II) based MOF formulations $[Cu_2(Glu)_2(μ\text{-}L)]xH_2O$ (Glu=-glutarate, L=4,4′-bipyridine (**1**), 1,2-bis(4-pyridyl)ethane (**2**), 1,2-bis(4--pyridyl)ethylene (**3**), and 1,2-bis(4-pyridyl)propane (**4**)), prepared by Jo et al., were shown to exert excellent antibacterial activities against *E. coli*, *S. aureus*, *K. pneumonia*, *P. aeruginosa*, and Methicillin -resistant *S. aureus* (MRSA) bacteria with the MBC values of 20 μg/mL for all bacterial strains [77]. In this study, the antimicrobial properties of the L-AA-Cu(II) MOFs were investigated against *E. coli* (gram -, ATCC 8739), *S. aureus* (gram +, ATCC 6538) and *C. albicans* (fungi, ATCC 10231) by micro-dilution method. The minimum inhibition concentration (MIC), and minimum bactericidal/fungicidal concentration (MBC/MFC) values of L-AA based Cu(II) MOFs prepared from different salts had been compared with each other and summarized in Table 2.

Gentamicin was used as a control in the experiment and MIC values of which against *E. coli, S. aureus* and *C. albicans* were reported to be 0.008 mg/mL, 0.01 mg/mL, and 0.0025 mg/mL, respectively [78–80]. L-AA based Cu(II) MOFs have shown considerable antibacterial and antifungal activity against indicated microorganisms. The L-AA-Cu(II)-C and L-AA-Cu(II)-N MOFs were shown to attain MIC values of 1.25 mg/mL for *E. coli* whereas L-AA-Cu(II)-A and L-AA-Cu(II)-S MOFs had lower MIC value as 0.63 mg/mL. MBC values of all types of L-AA-Cu(II) MOFs for *E. coli* were determined as 2.50 mg/mL. Moreover, L-AA-Cu(II)-C and L-AA-Cu(II)-S MOFs exhibited MIC values of 0.63 mg/mL against *S. aureus*, while L-AA-Cu(II)-A and L-AA-Cu(II)-N MOFs had 1.25 mg/mL. The MBC values for all types of L-AA-Cu(II) MOFs were determined as 2.50 mg/mL same as those for *E. coli*. The L-AA-Cu(II) MOFs were also

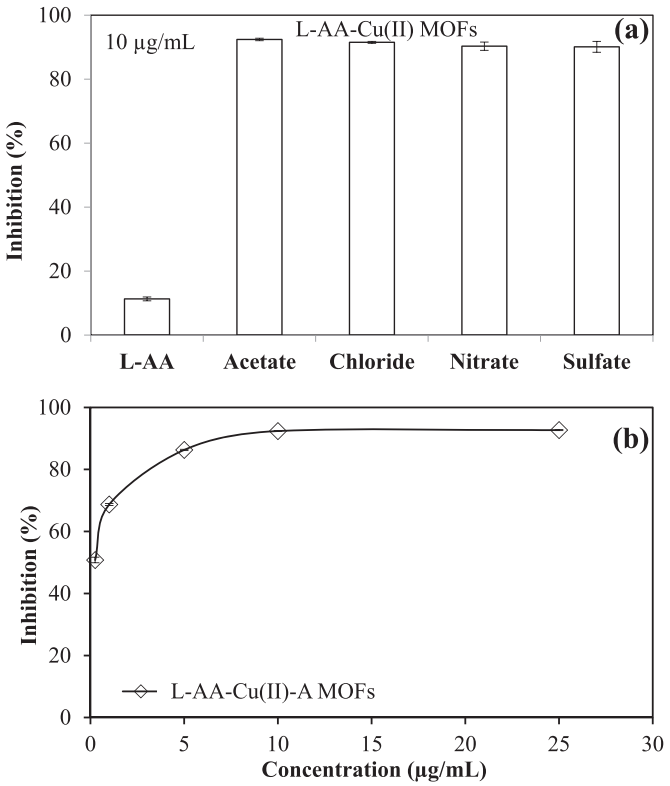

Fig. 5. **(a)** The α-Glucosidase inhibition activity of L-AA based Cu(II) MOFs at 10 µg/mL concentration, and **(b)** concentration dependent α-Glucosidase inhibitory activities of L-AA-Cu(II)-A MOFs from 0.25 to 25 µg/mL.

Table 2
MIC and MBC/MFC values of L-AA based Cu(II) MOFs against *E. coli* (gram -) and *S. aureus* (gram +) bacterial and *C. Albicans* fungal strains.

Organisms L-AA-Cu(II) MOFs	*E. coli*		*S. aureus*		*C. albicans*	
	MIC (mg/mL)	MBC (mg/mL)	MIC (mg/mL)	MBC (mg/mL)	MIC (mg/mL)	MFC (mg/mL)
A	0.63	2.50	1.25	2.50	1.25	2.50
C	1.25	2.50	0.63	2.50	2.50	2.50
N	1.25	2.50	1.25	2.50	2.50	2.50
S	0.63	2.50	0.63	2.50	1.25	2.50

shown to possess effective antifungal properties against *C. albicans* with slightly higher MIC values. MIC values of L-AA-Cu(II)-C and L-AA-Cu(II)-N MOFs were found to be 2.5 mg/mL on the other hand, L-AA-Cu(II)-A and L-AA-Cu(II)-S MOFs had lower MIC values with 1.25 mg/mL concentration. The MFC values of all types of L-AA based Cu(II) MOFs were determined as 2.50 mg/mL concentrations. The differences on the antimicrobial properties of L-AA based Cu(II) MOFs prepared from different metal precursors could be due to several factors e.g., differences in their surface areas and Cu(II) contents that might be affecting their engagement to microorganisms as well as the differences in the hydrogen bonding capabilities of counter ions i.e., acetate, chloride, nitrate, and sulfate salts of Cu(II)) [81] that may have also an effect on their interaction with the microorganisms [82].

3.4. Blood compatibility of L-AA-Cu(II) MOFs

Blood compatibility of nanomaterials is one of the crucial concerns in evaluation of their feasibility for biomedical applications [83]. Nanomaterials introduced into bloodstream are recognized as foreign object and will be coated by serum proteins including coagulation factors and inflammatory complement system components and induce a physiological response such as inflammation, hemolysis or stimulation of blood coagulation cascades depending upon the nature of materials [84–86]. Hemocompatibility of L-AA based Cu(II) MOFs were determined via *in vitro* hemolysis and blood clotting assays in order to evaluate their potential for biomedical applications requiring blood contact and the results were illustrated in Fig. 6 (a) and (b), respectively. Hemolysis induction of L-AA and L-AA-Cu(II)-A, -C, -N, -S MOFs at 1.0 µg/mL concentration are found to be 0.61 ± 0.20%, 0.43 ± 0.25%, 0.94 ± 0.24%, 0.91 ± 0.40%, 1.18 ± 0.10%, respectively. Based on these results L-AA based Cu(II) MOFs can be regarded as nonhemolytic at 1 µg/mL concentrations [87]. Considering the α-Glucosidase inhibitory activity of L-AA-Cu(II)-A MOFs as 68.7 ± 0.3% at this concentration and MIC values of respectively 0.63, 1.25 and 1.25 mg/mL against *E. coli, S. aureus*, and *C. albicans*, they can potentially be used as decent antidiabetic and antimicrobial materials with porous structures which could also be used to encapsulate supportive therapeutic agents.

Blood coagulation is a complex process of interconnected and stringently coordinated sequence of interactions between endothelium and coagulation factors also called “coagulation cascade” that involves intrinsic and extrinsic pathways [88]. Coagulation of blood is aimed to be a locally initiated process in a controlled manner. Activation of coagulation cascade in uncontrolled or undesired circumstances can lead to intravascular thrombi formation and may cause adverse/fatal consequences [83,88,89]. Due to complicated nature of reactions and amplification possibility in coagulation process even small alterations in natural functioning of blood components e.g., by foreign particles may stimulate coagulation [88,89]. In view of potential blood coagulative effects of L-AA based Cu(II) MOFs. In assessment of potential blood coagulative effects of L-AA based Cu(II) MOFs, *in vitro* blood clotting assay was conducted, and the results were given in Fig. 6 (b). As can be seen therefrom, blood clotting indices of L-AA, and L-AA based Cu(II) MOFs ranged from approximately 90 to 99% at 1 µg/mL concentrations specifically blood clotting indices were found as 87.18% ± 2.43, 89.31% ± 2.57, 99.91% ± 4.02, 91.17% ± 2.31, and 98.7%1 ± 3.22 respectively for bare L-AA, and L-AA-Cu(II)-A, L-AA-Cu(II)-C, L-AA-Cu(II)-N, and

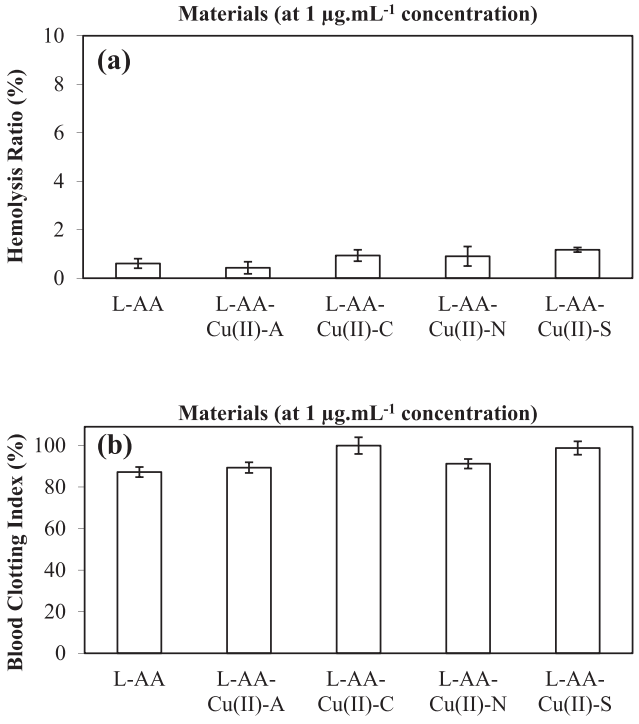

Fig. 6. The assessment of hemocompatibility of the L-AA-Cu(II) MOFs via **(a)** hemolysis and **(b)** blood clotting assays.

L-AA-Cu(II)-S MOFs, highlighting that they did not induce significant coagulation in comparison to control group [53]. Consequently, from hemocompatibility studies, L-AA based Cu(II) MOFs have revealed to be non-hemolytic and non-coagulative at 1 μg/mL concentrations thus can be considered as safe to come into contact with blood in terms of tested parameters. However, further research should be devoted obtaining safety dosage margins of these materials for *in vivo* applications.

4. Conclusion

L-AA based Cu(II)-A, -C, -N, and -S MOFs successfully synthesized in this study with 40.5 ± 2.1, 50.8 ± 1.9, 40.2 ± 1.6, and 36.8 ± 1.3%, gravimetric yields and specific surface areas of respectively 96.7 ± 2.4, 89.8 ± 3.1, 92.1 ± 1.5 and 74.6 ± 5.2 m^2/g have shown to exert decent biological utilization. Bio-MOFs were shown to be generated by coordination of Cu(II) ions and L-AA from its carboxylic acid groups and formed rod-like assemblies with hexagonal crystallization patterns as revealed by XRD analysis and computational modelling thereof. Antimicrobial activity of Cu(II) ions [90] has been inherited into L-AA based Cu(II) MOFs, hence are anticipated to be primary drivers of their antibacterial and antifungal activity against *E. coli* ATCC 8739, *S. aureus* ATCC 6538, *C. albicans* with the MIC values of as low as 0.63–1.25 mg/mL for bacterial and 1.25–2.50 mg/mL for fungal strains, respectively. Moreover, L-AA amino acids found in the catalytic domain of α-Glucosidase enzyme [73] has been presumed to be main cause of inhibitory activities of L-AA based Cu(II) MOFs through interacting with Cu(II) ions in their structure. However, more elaborate analyses should be committed to determine exact mode of action underlying their inhibitory effects on α-Glucosidase enzyme. Hemocompatibility of L-AA based Cu(II) MOFs assessed by *in vitro* hemolysis and blood clotting assays suggest their safety at 1 μg/mL concentration for applications involving direct contact with whole blood e.g., hemodialysis, drug delivery, and so forth. However, a more detailed analyses ought to be devoted on determining suitable dosage ranges before intending implementation of L-AA based Cu(II) MOFs for *in vivo* studies. As it is evidenced by the improvements in biomedicine, greener energy applications, and industrial processes based in designing multifunctional micro/nano interfaces, safe and green materials in from natural and sustainable source are of significant importance. In this context, MOFs designed from natural biocompatible and renewable precursors, holds great promise as porous and high surface interfaces with feasibility to vast array of biomedical and industrial applications.

CRediT authorship contribution statement

Gorkem Gizer: Formal analysis, Investigation, Methodology, Writing – original draft. **Mehtap Sahiner:** Formal analysis, Investigation, Methodology, Writing – original draft. **Yildiz Yildirim:** Formal analysis, Investigation, Data curation, Writing – original draft. **Sahin Demirci:** Formal analysis, Investigation, Validation, Methodology, Writing – original draft. **Mehmet Can:** Formal analysis, Investigation, Validation, Writing – original draft. **Nurettin Sahiner:** Conceptualization, Formal analysis, Investigation, Methodology, Funding acquisition, Visualization, Resources, Supervision, Writing – review & editing.

Declaration of competing interest

The authors declare that they have no known competing financial interests or personal relationships that could have appeared to influence the work reported in this paper.

Appendix A. Supplementary data

Supplementary data to this article can be found online at https://doi.org/10.1016/j.crgsc.2021.100110.

References

[1] H. Furukawa, K.E. Cordova, M. O'Keeffe, O.M. Yaghi, The chemistry and applications of metal-organic frameworks,, Science 341 (2013), https://doi.org/10.1126/science.1230444.

[2] N. Hanikel, M.S. Prévot, O.M. Yaghi, MOF water harvesters, Nat. Nanotechnol 15 (2020) 348–355, https://doi.org/10.1038/s41565-020-0673-x.

[3] S.L. Anderson, K.C. Stylianou, Biologically derived metal organic frameworks, Coord. Chem. Rev. 349 (2017) 102–128, https://doi.org/10.1016/j.ccr.2017.07.012.

[4] R.R. Salunkhe, Y.V. Kaneti, Y. Yamauchi, Metal-organic framework-derived nanoporous metal oxides toward supercapacitor applications: progress and prospects, ACS, Nano 11 (2017) 5293–5308, https://doi.org/10.1021/acsnano.7b02796.

[5] C.J. Doonan, C.J. Sumby, Metal-organic framework catalysis, CrystEngComm 19 (2017) 4045–4049, https://doi.org/10.1039/c7ce90106b.

[6] M. Ding, R.W. Flaig, H.L. Jiang, O.M. Yaghi, Carbon capture and conversion using metal-organic frameworks and MOF-based materials, Chem. Soc. Rev. 48 (2019) 2783–2828, https://doi.org/10.1039/c8cs00829a.

[7] S. Ma, H.C. Zhou, Gas storage in porous metal-organic frameworks for clean energy applications, Chem. Commun. 46 (2010) 44–53, https://doi.org/10.1039/b916295j.

[8] K. Cheng, Y. Li, Z. Gao, F. Chen, C. You, B. Sun, Two-dimensional metal organic framework for effective gas absorption, Inorg. Chem. Commun. 101 (2019) 27–31, https://doi.org/10.1016/j.inoche.2018.12.003.

[9] Z.R. Herm, B.M. Wiers, J.A. Mason, J.M. Van Baten, M.R. Hudson, P. Zajdel, C.M. Brown, N. Masciocchi, R. Krishna, J.R. Long, Separation of hexane isomers in a metal-organic framework with triangular channels, Science 340 (2013) 960–964, https://doi.org/10.1126/science.1234071.

[10] J. Chang, X. Wang, J. Wang, H. Li, F. Li, Nucleic acid-functionalized metal-organic framework-based homogeneous electrochemical biosensor for simultaneous detection of multiple tumor biomarkers, Anal. Chem. 91 (2019) 3604–3610, https://doi.org/10.1021/acs.analchem.8b05599.

[11] H.-S. Wang, Metal–organic frameworks for biosensing and bioimaging applications, Coord. Chem. Rev. 349 (2017) 139–155, https://doi.org/10.1016/j.ccr.2017.08.015.

[12] W. Cai, J. Wang, C. Chu, W. Chen, C. Wu, G. Liu, Metal–organic framework-based stimuli-responsive systems for drug delivery, Adv. Sci. 6 (2019), https://doi.org/10.1002/advs.201801526.

[13] A. Roshan, C. Joseph, M.A. Ittyachen, Growth and characterization of a new metal-organic crystal: potassium thiourea bromide, Mater. Lett. 49 (2001) 299–302, https://doi.org/10.1016/S0167-577X(00)00388-8.

[14] J.D. Xiao, L.G. Qiu, F. Ke, Y.P. Yuan, G.S. Xu, Y.M. Wang, X. Jiang, Rapid synthesis of nanoscale terbium-based metal-organic frameworks by a combined ultrasound-vapour phase diffusion method for highly selective sensing of picric acid, J. Mater. Chem. 1 (2013) 8745–8752, https://doi.org/10.1039/c3ta11517h.

[15] J. Wang, X. Luo, C. Young, J. Kim, Y.V. Kaneti, J. You, Y.M. Kang, Y. Yamauchi, K.C.W. Wu, A glucose-assisted hydrothermal reaction for directly transforming metal-organic frameworks into hollow carbonaceous materials,, Chem. Mater. 30 (2018) 4401–4408, https://doi.org/10.1021/acs.chemmater.8b01792.

[16] R. Sen, D. Saha, S. Koner, Controlled construction of metal-organic frameworks: hydrothermal synthesis, X-ray structure, and heterogeneous catalytic study, Chem, Eur. J. 18 (2012) 5979–5986, https://doi.org/10.1002/chem.201102953.

[17] E. Haque, N.A. Khan, H.J. Park, S.H. Jhung, Synthesis of a metal-organic framework material, iron terephthalate, by ultrasound, microwave, and conventional electric heating: a kinetic study, Chem. Eur. J. 16 (2010) 1046–1052, https://doi.org/10.1002/chem.200902382.

[18] H.S. Wang, Y.H. Wang, Y. Ding, Development of biological metal-organic frameworks designed for biomedical applications: from bio-sensing/bio-imaging to disease treatment, Nanoscale Adv 2 (2020) 3788–3797, https://doi.org/10.1039/d0na00557f.

[19] I. Imaz, M. Rubio-Martínez, J. An, I. Solé-Font, N.L. Rosi, D. Maspoch, Metal–biomolecule frameworks (MBioFs), Chem. Commun. 47 (2011) 7287, https://doi.org/10.1039/c1cc11202c.

[20] R.A. Smaldone, R.S. Forgan, H. Furukawa, J.J. Gassensmith, A.M.Z. Slawin, O.M. Yaghi, J.F. Stoddart, Metal-organic frameworks from edible natural products, in: Angew Chemie Int (Ed.) 49, 2010, pp. 8630–8634, https://doi.org/10.1002/anie.201002343.

[21] E. Yang, L. Wang, F. Wang, Q. Lin, Y. Kang, J. Zhang, Zeolitic metal–organic frameworks based on amino acid, Inorg. Chem. 53 (2014) 10027–10029, https://doi.org/10.1021/ic501556w.

[22] R. Ferrari, S. Bernes, C.R. de Barbarín, G. Mendoza-Díaz, L. Gasque, Interaction between Glyglu and Ca2+, Pb2+, Cd2+ and Zn2+ in solid state and aqueous solution., Inorganica Chim, Acta 339 (2002) 193–201, https://doi.org/10.1016/S0020-1693(02)01047-2.

[23] A. Mantion, L. Massüger, P. Rabu, C. Palivan, L.B. McCusker, A. Taubert, Metal−Peptide frameworks (MPFs): "bioinspired" metal organic frameworks, J. Am. Chem. Soc. 130 (2008) 2517–2526, https://doi.org/10.1021/ja0762588.

[24] J. Navarro-Sánchez, A.I. Argente-García, Y. Moliner-Martínez, D. Roca-Sanjuán, D. Antypov, P. Campíns-Falcó, M.J. Rosseinsky, C. Martí-Gastaldo, Peptide metal–organic frameworks for enantioselective separation of chiral drugs, J. Am. Chem. Soc. 139 (2017) 4294–4297, https://doi.org/10.1021/jacs.7b00280.

[25] Y. Rachuri, J.F. Kurisingal, R.K. Chitumalla, S. Vuppala, Y. Gu, J. Jang, Y. Choe, E. Suresh, D.-W. Park, Adenine-based Zn(II)/Cd(II) metal–organic frameworks as efficient heterogeneous catalysts for facile CO 2 fixation into cyclic carbonates: a

DFT-supported study of the reaction mechanism,, Inorg. Chem. 58 (2019) 11389–11403, https://doi.org/10.1021/acs.inorgchem.9b00814.
[26] J. An, S.J. Geib, N.L. Rosi, Cation-triggered drug release from a porous Zinc−Adeninate Metal−Organic framework, J. Am. Chem. Soc. 131 (2009) 8376–8377, https://doi.org/10.1021/ja902972w.
[27] J.P. García-Terán, O. Castillo, A. Luque, U. García-Couceiro, P. Román, L. Lezama, An unusual 3D coordination polymer based on bridging interactions of the nucleobase adenine, Inorg. Chem. 43 (2004) 4549–4551, https://doi.org/10.1021/ic049512v.
[28] M. Ismail, M.A. Bustam, Y.F. Yeong, Gallate-based metal–organic frameworks, a new family of hybrid materials and their applications: a review,, Crystals 10 (2020) 1006, https://doi.org/10.3390/cryst10111006.
[29] Z. Lin, J. Zhou, C. Cortez-Jugo, Y. Han, Y. Ma, S. Pan, E. Hanssen, J.J. Richardson, F. Caruso, Ordered mesoporous metal–phenolic network particles, J. Am. Chem. Soc. 142 (2020) 335–341, https://doi.org/10.1021/jacs.9b10835.
[30] Y. Ju, J. Cui, M. Müllner, T. Suma, M. Hu, F. Caruso, Engineering low-fouling and pH-degradable capsules through the assembly of metal-phenolic networks, Biomacromolecules 16 (2015) 807–814, https://doi.org/10.1021/bm5017139.
[31] M.A. Rahim, K. Kempe, M. Müllner, H. Ejima, Y. Ju, M.P. van Koeverden, T. Suma, J.A. Braunger, M.G. Leeming, B.F. Abrahams, F. Caruso, Surface-confined amorphous films from metal-coordinated simple phenolic ligands, chem. Mater. 27 (2015) 5825–5832, https://doi.org/10.1021/acs.chemmater.5b02790.
[32] S.A.A. Sajadi, Metal ion-binding properties of L-glutamic acid and L-aspartic acid, a comparative investigation, Nat. Sci. (2010) 85–90, https://doi.org/10.4236/ns.2010.22013, 02.
[33] O. Yamauchi, A. Odani, M. Takani, Metal–amino acid chemistry. Weak interactions and related functions of side chain groups, J. Chem. Soc., Dalton Trans. (2002) 3411–3421, https://doi.org/10.1039/B202385G.
[34] G.S. Jeong, A.C. Kathalikkattil, R. Babu, Y.G. Chung, D.W. Park, Cycloaddition of CO2 with epoxides by using an amino-acid-based Cu(II)–tryptophan MOF catalyst, Chin. J. Catal. 39 (2018) 63–70, https://doi.org/10.1016/S1872-2067(17)62916-4.
[35] M. Can, S. Demirci, A.K. Sunol, N. Sahiner, An amino acid, L-Glutamic acid-based metal-organic frameworks and their antibacterial, blood compatibility, biocompatibility, and sensor properties, Microporous Mesoporous Mater 309 (2020), 110533, https://doi.org/10.1016/j.micromeso.2020.110533.
[36] J.M. Schveigkardt, A.C. Rizzi, O.E. Piro, E.E. Castellano, R.C. de Santana, R. Calvo, C.D. Brondino, Structural, Single Crystal, EPR studies of the complex copper L-glutamine: a weakly exchange-coupled system with syn-anti carboxylate bridges, Eur. J. Inorg. Chem. (2002) 2913–2919, https://doi.org/10.1002/1099-0682(200211)2002:11<2913::AID-EJIC2913>3.0.CO;2-P, 2002.
[37] F. Luo, Y. Yang, Y. Che, J. Zheng, Construction of Cu(II)–Gd(III) metal–organic framework by the introduction of a small amino acid molecule: hydrothermal synthesis, structure, thermostability, and magnetic studies, CrystEngComm 10 (2008) 1613, https://doi.org/10.1039/b808464e.
[38] B. Zhou, N.J.O. Silva, F.N. Shi, F. Palacio, L. Mafra, J. Rocha, Co II/Zn II-(L-tyrosine) magnetic metal-organic frameworks, Eur. J. Inorg. Chem. (2012) 5259–5268, https://doi.org/10.1002/ejic.201200169.
[39] Y.-X. Tan, Y.-P. He, J. Zhang, Serine-based homochiral nanoporous frameworks for selective CO 2 uptake, Inorg. Chem. 50 (2011) 11527–11531, https://doi.org/10.1021/ic201442u.
[40] K. Stenzel, M. Fleck, Poly[[[diaquacobalt(II)]-di-μ-glycine] dichloride], acta crystallogr. Sect. E struct 60 (2004) m1470–m1472, https://doi.org/10.1107/S1600536804022573. Reports Online.
[41] J.H. Zhang, R.Y. Nong, S.M. Xie, B.J. Wang, P. Ai, L.M. Yuan, Homochiral metal-organic frameworks based on amino acid ligands for HPLC separation of enantiomers, Electrophoresis 38 (2017) 2513–2520, https://doi.org/10.1002/elps.201700122.
[42] S. Wang, M. Wahiduzzaman, L. Davis, A. Tissot, W. Shepard, J. Marrot, C. Martineau-Corcos, D. Hamdane, G. Maurin, S. Devautour-Vinot, C. Serre, A robust zirconium amino acid metal-organic framework for proton conduction, Nat, Commun. Now. 9 (2018) 1–8, https://doi.org/10.1038/s41467-018-07414-4.
[43] S. Pabba, A. Kumari, M.G. Ravuri, P.K. Thella, B. Satyavathi, K. Shah, S. Kundu, S.K. Bhargava, Experimental determination and modelling of the co-solvent and antisolvent behaviour of binary systems on the dissolution of pharma drug; L-aspartic acid and thermodynamic correlations, J. Mol. Liq 314 (2020), 113657, https://doi.org/10.1016/j.molliq.2020.113657.
[44] B.L. Kreamer, F.L. Siegel, G.R. Gourley, A novel inhibitor of β-glucuronidase: l-aspartic acid,, Pediatr. Res. 50 (2001) 460–466, https://doi.org/10.1203/00006450-200110000-00007.
[45] H. Koyuncuoğlu, E. Genç, M. Güngör, L. Eroğlu, H. Saǧduyu, The antagonizing effect of aspartic acid on the brain levels of monoamines and free amino acids during the development of tolerance to and physical dependence on morphine,, Psychopharmacology (Berlin) 54 (1977) 187–191, https://doi.org/10.1007/BF00426778.
[46] H. Koyuncuoğlu, The treatment with dextromethorphan of heroin addicts, in: N. Loimer, R. Schmid, A. Springer, 1991, pp. 320–329, https://doi.org/10.1007/978-3-7091-9173-6_38. Drug Addict. AIDS, 1st ed., Springer Vienna, Vienna,.
[47] J. Gao, D. Lv, H. Sun, W. Yang, Determination of L-aspartic acid by using the Cu(II)-catalyzed oscillating reaction, J. Braz. Chem. Soc. 20 (2009) 1827–1832, https://doi.org/10.1590/S0103-50532009001000009.
[48] K. Nomiya, H. Yokoyama, Syntheses, crystal structures and antimicrobial activities of polymeric silver(i) complexes with three amino-acids [aspartic acid (H2asp), glycine (Hgly) and asparagine (Hasn)]Note: for ease of reference during discussion of their anions, H2asp, Hgly and, J. Chem. Soc. Dalt. Trans (2002) 2483–2490, https://doi.org/10.1039/b200684g.
[49] T. Komiyama, S. Igarashi, Y. Yukawa, Synthesis of polynuclear complexes with an amino acid or a peptide as a bridging ligand, Curr. Chem. Biol. 2 (2008) 122–139, https://doi.org/10.2174/187231308784220509.
[50] N. Sahiner, K. Sel, O.F. Ozturk, S. Demirci, G. Terzi, Facile synthesis and characterization of trimesic acid-Cu based metal organic frameworks, Appl. Surf. Sci. 314 (2014) 663–669, https://doi.org/10.1016/j.apsusc.2014.07.023.
[51] Z. Wang, K. Wang, Y. Feng, S. Jiang, Y. Zhao, M. Zeng, Preparation, characterization of L-aspartic acid chelated calcium from oyster shell source and its calcium supplementation effect in rats, J. Funct. Foods 75 (2020), 104249, https://doi.org/10.1016/j.jff.2020.104249.
[52] S. Demirci, N. Sahiner, Superporous neutral, anionic, and cationic cryogel reactors to improved enzymatic activity and stability of α-Glucosidase enzyme via entrapment method, Chem. Eng. J 409 (2021), 128233, https://doi.org/10.1016/j.cej.2020.128233.
[53] N. Sahiner, S. Sagbas, N. Aktas, C. Silan, Inherently antioxidant and antimicrobial tannic acid release from poly(tannic acid) nanoparticles with controllable degradability, Colloids Surf. B Biointerfaces 142 (2016) 334–343, https://doi.org/10.1016/j.colsurfb.2016.03.006.
[54] Y. Zhao, Y. Wang, F. Ran, Y. Cui, C. Liu, Q. Zhao, Y. Gao, D. Wang, S. Wang, A comparison between sphere and rod nanoparticles regarding their in vivo biological behavior and pharmacokinetics,, Sci. Rep. 7 (2017) 1–11, https://doi.org/10.1038/s41598-017-03834-2.
[55] R.M. Mutiso, M.C. Sherrott, A.R. Rathmell, B.J. Wiley, K.I. Winey, Integrating simulations and experiments to predict sheet resistance and optical transmittance in nanowire films for transparent conductors, ACS Nano 7 (2013) 7654–7663, https://doi.org/10.1021/nn403324t.
[56] M.J.A. Hore, R.J. Composto, Functional polymer nanocomposites enhanced by nanorods, Macromolecules 47 (2014) 875–887, https://doi.org/10.1021/ma402179w.
[57] A. Abdulkareem Ghassan, N.-A. Mijan, Y. Hin Taufiq-Yap, Nanomaterials: an overview of nanorods synthesis and optimization, Nanorods Nanocomposites (2020), https://doi.org/10.5772/intechopen.84550.
[58] J.T.L. Navarrete, V. Hernández, F.J. Ramírez, Ir and Raman spectra of L-aspartic acid and isotopic derivatives, Biopolymers 34 (1994) 1065–1077, https://doi.org/10.1002/bip.360340810.
[59] A.J. Howarth, Y. Liu, P. Li, Z. Li, T.C. Wang, J.T. Hupp, O.K. Farha, Chemical, thermal and mechanical stabilities of metal–organic frameworks, Nat. Rev. Mater 1 (2016), 15018, https://doi.org/10.1038/natrevmats.2015.18.
[60] K. Tao, X. Han, Q. Yin, D. Wang, L. Han, L. Chen, Metal-organic frameworks-derived porous In2O3 hollow nanorod for high-performance ethanol gas sensor, Chemistry 2 (2017) 10918–10925, https://doi.org/10.1002/slct.201701752.
[61] Z.A. Alothman, A review: fundamental aspects of silicate mesoporous materials,, Materials 5 (2012) 2874–2902, https://doi.org/10.3390/ma5122874.
[62] F. Zhu, T. Asada, A. Sato, Y. Koi, H. Nishiwaki, H. Tamura, Rosmarinic acid extract for antioxidant, antiallergic, and α-glucosidase inhibitory activities, isolated by supramolecular technique and solvent extraction from Perilla leaves, J. Agric. Food Chem. 62 (2014) 885–892, https://doi.org/10.1021/jf404318j.
[63] M.S. Hedrington, S.N. Davis, Considerations when using alpha-glucosidase inhibitors in the treatment of type 2 diabetes, Expert Opin, Pharmacother 20 (2019) 2229–2235, https://doi.org/10.1080/14656566.2019.1672660.
[64] U.F. Magaji, O. Sacan, R. Yanardag, Alpha amylase, alpha glucosidase and glycation inhibitory activity of Moringa oleifera extracts, South African J. Bot. 128 (2020) 225–230, https://doi.org/10.1016/j.sajb.2019.11.024.
[65] T.M. Costa, D.A. Mayer, D.A. Siebert, G.A. Micke, M.D. Alberton, L.B.B. Tavares, D. de Oliveira, Kinetics analysis of the inhibitory effects of alpha-glucosidase and identification of compounds from ganoderma lipsiense mycelium, Appl. Biochem. Biotechnol. 191 (2020) 996–1009, https://doi.org/10.1007/s12010-020-03239-4.
[66] K.P. Mugaranja, A. Kulal, Alpha glucosidase inhibition activity of phenolic fraction from Simarouba glauca: an in-vitro, in-silico and kinetic study, Heliyon 6 (2020), e04392, https://doi.org/10.1016/j.heliyon.2020.e04392.
[67] P.O. Fayemi, I. Ozturk, D. Kaan, S. Özcan, M.B. Yerer, A.H. Dokumaci, C. Özcan, G.E. Uwaya, O.E. Fayemi, H. Yetim, Bioactivities of phytochemicals in Callistemon citrinus against multi-resistant foodborne pathogens, alpha glucosidase inhibition and MCF-7 cancer cell line, Biotechnol. Biotechnol. Equip. 33 (2019) 764–778, https://doi.org/10.1080/13102818.2019.1616615.
[68] Y. Li, Z. Fu, G. Xu, Metal-organic framework nanosheets: preparation and applications, Coord. Chem. Rev. 388 (2019) 79–106, https://doi.org/10.1016/j.ccr.2019.02.033.
[69] M. Xu, S. Yuan, X.-Y. Chen, Y.-J. Chang, G. Day, Z.-Y. Gu, H.-C. Zhou, Two-dimensional metal–organic framework nanosheets as an enzyme inhibitor: modulation of the α-chymotrypsin activity, J. Am. Chem. Soc. 139 (2017) 8312–8319, https://doi.org/10.1021/jacs.7b03450.
[70] N.J. Shamle, A.C. Tella, J.A. Obaleye, F.O. Balogun, A.O.T. Ashafa, P.A. Ajibade, Synthesis, characterization, antioxidant and antidiabetic studies of Cu(II) and Zn(II) complexes of tolfenamic acid/mefenamic acid with 1-methylimidazole, Inorganica Chim. Acta 513 (2020), 119942, https://doi.org/10.1016/j.ica.2020.119942.
[71] Y. Yoshikawa, R. Hirata, H. Yasui, H. Sakurai, Alpha-glucosidase inhibitory effect of anti-diabetic metal ions and their complexes, Biochimie 91 (2009) 1339–1341, https://doi.org/10.1016/j.biochi.2009.06.005.
[72] D. Avcı, S. Altürk, F. Sönmez, Ö. Tamer, A. Başoğlu, Y. Atalay, B.Z. Kurt, N. Dege, Novel Cu(II), Co(II) and Zn(II) metal complexes with mixed-ligand: synthesis, crystal structure, α-glucosidase inhibition, DFT calculations, and molecular docking, J. Mol. Struct. 1197 (2019) 645–655, https://doi.org/10.1016/j.molstruc.2019.07.039.
[73] N.S.H.N. Moorthy, M.J. Ramos, P.A. Fernandes, Studies on α-glucosidase inhibitors development: magic molecules for the treatment of carbohydrate mediated

diseases, Mini Rev. Med. Chem. 12 (2012) 713–720, https://doi.org/10.2174/138955712801264837.
[74] W. Lestari, R.T. Dewi, L.B.S. Kardono, A. Yanuar, Docking Sulochrin, Its Derivative, As α-glucosidase inhibitors of *Saccharomyces cerevisiae*, indones. J. Chem. 17 (2017) 144, https://doi.org/10.22146/ijc.23568.
[75] Z. Ozturk, D.A. Kose, A. Asan, G. Ozkan, Porous metal-organic Cu(II) complex of L-Arginine; synthesis, characterization, hydrogen storage properties and molecular simulation calculations, Hittite J. Sci. Eng 1 (2015) 1–5, https://doi.org/10.17350/HJSE19030000001.
[76] R. Karimi Alavijeh, S. Beheshti, K. Akhbari, A. Morsali, Investigation of reasons for metal–organic framework's antibacterial activities, Polyhedron 156 (2018) 257–278, https://doi.org/10.1016/j.poly.2018.09.028.
[77] J.H. Jo, H.C. Kim, S. Huh, Y. Kim, D.N. Lee, Antibacterial activities of Cu-MOFs containing glutarates and bipyridyl ligands, Dalton Trans. 48 (2019) 8084–8093, https://doi.org/10.1039/c9dt00791a.
[78] S. Helmy, S.S. Mohamed, S.S. Mahmoud, M. Talaat, Preparation and characterization of DMPC liposomal-gentamicin; antibacterial time-kill study on Escherichia coli ATCC 8739, Int. J. Innov. Sci. Eng. Technol 3 (2015) 221–224.
[79] A.M. Leite, E.D.O. Lima, E.L. De Souza, M.D.F.F.M. Diniz, V.N. Trajano, I.A. De Medeiros, Inhibitory effect of β-pinene, α-pinene and eugenol on the growth of potential infectious endocarditis causing Gram-positive bacteria, Rev. Bras. Ciencias Farm, J. Pharm. Sci. 43 (2007) 121–126, https://doi.org/10.1590/S1516-93322007000100015.
[80] M. Lu, C. Yu, X. Cui, J. Shi, L. Yuan, S. Sun, Gentamicin synergises with azoles against drug-resistant Candida albicans, Int. J. Antimicrob. Agents 51 (2018) 107–114, https://doi.org/10.1016/j.ijantimicag.2017.09.012.
[81] S.J. Pike, J.J. Hutchinson, C.A. Hunter, H-bond acceptor parameters for anions, J. Am. Chem. Soc. 139 (2017) 6700–6706, https://doi.org/10.1021/jacs.7b02008.
[82] D. Chen, N. Oezguen, P. Urvil, C. Ferguson, S.M. Dann, T.C. Savidge, Regulation of protein-ligand binding affinity by hydrogen bond pairing, Sci. Adv 2 (2016), e1501240, https://doi.org/10.1126/sciadv.1501240.
[83] M. Weber, H. Steinle, S. Golombek, L. Hann, C. Schlensak, H.P. Wendel, M. Avci-Adali, Blood-contacting biomaterials: in vitro evaluation of the hemocompatibility, Front. Bioeng. Biotechnol 6 (2018), https://doi.org/10.3389/fbioe.2018.00099.
[84] D.F. Williams, On the mechanisms of biocompatibility, Biomaterials 29 (2008) 2941–2953, https://doi.org/10.1016/j.biomaterials.2008.04.023.
[85] B. Nilsson, K.N. Ekdahl, T.E. Mollnes, J.D. Lambris, The role of complement in biomaterial-induced inflammation,, Mol. Immunol. 44 (2007) 82–94, https://doi.org/10.1016/j.molimm.2006.06.020.
[86] M.B. Gorbet, M.V. Sefton, Biomaterial-associated thrombosis: roles of coagulation factors, complement, platelets and leukocytes, Biomaterials 25 (2004) 5681–5703, https://doi.org/10.1016/j.biomaterials.2004.01.023.
[87] D. Archana, J. Dutta, P.K. Dutta, Evaluation of chitosan nano dressing for wound healing: characterization, in vitro and in vivo studies, Int. J. Biol. Macromol. 57 (2013) 193–203, https://doi.org/10.1016/j.ijbiomac.2013.03.002.
[88] J. Hong, A. Larsson, K.N. Ekdahl, G. Elgue, R. Larsson, B. Nilsson, Contact between a polymer and whole blood: sequence of events leading to thrombin generation, J. Lab. Clin. Med. 138 (2001) 139–145, https://doi.org/10.1067/mlc.2001.116486.
[89] R.M. Jay, P. Lui, How anticoagulants work, Tech. Reg. Anesth. Pain Manag. 10 (2006) 30–39, https://doi.org/10.1053/j.trap.2006.04.002.
[90] M. Rosenberg, H. Vija, A. Kahru, C.W. Keevil, A. Ivask, Rapid in situ assessment of Cu-ion mediated effects and antibacterial efficacy of copper surfaces, Sci. Rep 8 (2018) 8172, https://doi.org/10.1038/s41598-018-26391-8.